Chapter 5
Fatigue Assessment of Porosity in Electron Beam Melted Ti-6Al-4V

Justin Warner, Dino Celli, Jacob Rindler, M. Herman Shen, Onome Scott-Emuakpor, and Tommy George

Abstract Additive manufacturing (AM) has proven itself to be an effective and versatile solution in replacing aircraft structures and components. However, the AM process still requires the necessary structural reliability as well as the technology to assess operational longevity. In this work, a fatigue performance and damage progression assessment framework is proposed to achieve a fundamental understanding of the fatigue damage mechanisms and its progression in as-built treated electron beam melted (EBM) Ti-6Al-4V at the macroscopic structural scale as well as at the microscopic constituent scale. The work presented utilizes digital image correlation (DIC), an optical strain measurement technique, as a method to detect crack initiation sites occurring on the material's surface and propagating throughout the specimen. A comprehensive testing framework and experimental procedure is developed to generate fatigue data for AM material Ti-6Al-4V as-built specimens. Characterization and simulation of the fatigue progress due to AM process defects (voids, surface roughness, etc.) are also performed using damaging energy progress and damage evaluation.

Keywords Fatigue · Porosity · Computed tomography · Defect damage criterion · Digital image correlation

Many research efforts, within the engineering community, have been focused on the improvement of additive manufactured (AM) materials. Specifically, the fatigue life characterization is of great interest to the aerospace industry due to high standards for the fatigue performance of materials in flight critical components. Powder bed fusion(PBF) is a commonly used AM process to produce components within a small region (200–350 mm) of space by using thermal energy to fuse powder and build a product [1]. There are various options when considering which PBF method to use (i.e., electron beam melting, direct metal laser sintering, selective laser sintering/melting). Electron beam melting (EBM) is an accepted method that is relatively inexpensive and has a small footprint by recycling the unused powder [1]. EBM uses an electron beam source, which can create internal stress-concentrating defects, such as porosity, and significantly reduces fatigue life. This becomes significantly more important for the aerospace industry as fatigue of engineering components made up 25% of all failures and 55% in aircraft components [2]. Therefore, to utilize AM materials for aerospace components, characterizing and ultimately reducing defects within AM materials such as Ti-6Al-4V, Inconel 718, and Aluminum 7075 are demanded to ensure proper safety standards.

Various parameterized defect detriment criterions are investigated to identify the crack initiation site which ultimately leads to fatigue failure. 3D computed tomography (CT) scan data was completed to use identified individual defects characteristics to distinguish fatigue life performance. This was conducted in effort to develop a cycle to failure fatigue life prediction and locates the area of interest of crack initiation prior to destructive testing. Detecting the initiation site can aid in the AM process by informing, via in situ (QM meltpool) or post-CT scans, defect attributes without destructive testing. In addition to determining actual cycles to failure, defect attributes were identified for life prediction with CDM or fracture mechanic fatigue life approaches. Digital image correlation (DIC), an optical strain measurement technique, was used to aid in detection of the location of failure and strains fields. DIC data was utilized to cross-examine the dog bone specimen's regions of interest and evaluate defect detriment criterions' validity. Ti-6Al-4V was analyzed due to its wide application

J. Warner · D. Celli (✉) · J. Rindler · M. H. Shen
The Ohio State University, Columbus, OH, USA
e-mail: warner.799@osu.edu; warner.799@buckeyemail.osu.edu; celli.6@osu.edu; rindler.115@osu.edu; shen.1@osu.edu

O. Scott-Emuakpor · T. George
Air Force Research Laboratory, Wright-Patterson AFB, OH, USA
e-mail: onome.scott-emuakpor.1@us.af.mil; tommy.george@us.af.mil

S. Xia et al. (eds.), *Fracture, Fatigue, Failure and Damage Evolution, Volume 3*, Conference Proceedings of the Society for Experimental Mechanics Series, https://doi.org/10.1007/978-3-030-60959-7_5

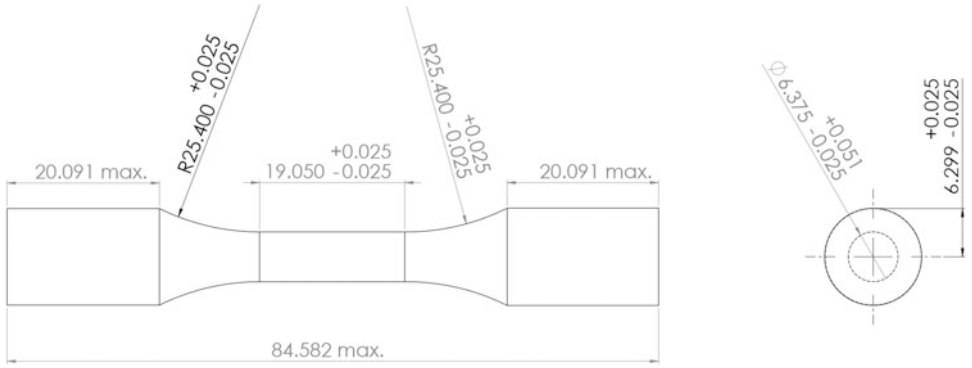

Fig. 5.1 Dimensions of specimen

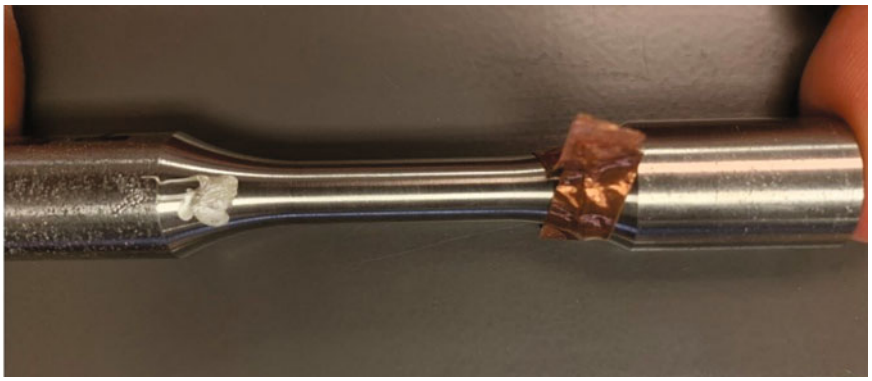

Fig. 5.2 Machined specimen with paste and tape

within the aerospace field. Recent work has shown hot isostatic pressing (HIPing) of Ti-6Al-4V reduces original diameter of void size, thus increasing AM material fatigue life by 20% [3]. Within this document, a porosity analysis has been conducted to examine the effects of the internal voids from a microscopic perspective.

5.1 Method

Materials for testing were obtained from the Center for Design and Manufacturing Excellence (CDME) at The Ohio State University. Ten Ti-6Al-4V cylindrical rods, with a height and diameter of approximately 174 and 13 mm, respectively, were additively manufactured with a vertical build layout using GE Arcam Q10+ Electron Beam system. Built on 1 -mm-high supports, the cylindrical rods were randomly distributed throughout the build chamber. The processing parameters were standard OEM Ti-6Al-4V proprietary melt and support themes for control software 5.2.1. The +45-105 µm recycled plasma atomized powder (AP&C) used for the build was all sourced from a singular lot with manufacturer reported chemistry; the number of powder reuses was not tracked (Fig. 5.1).

The rods were machined to the specified parameters shown in Fig. 5.2 with the result shown in Fig. 5.3. CT scans were performed by the Air Force Institute of Technology (AFIT). Specimen labeled 07-TT had a voxel size of 16.49 µm, and all other specimens reported had a voxel size of 14.911 µm. The CT scanner used to obtain the image data sets was the Nikon XT H 225 ST, with the standard settings used. In order to properly orient CT data to DIC, silver conductive paste was applied to the radius of the specimen. Copper tape was applied to the bottom radius for precompensation of beam hardening. CT data was then post-processed in ImageJ, an open architecture software for image data manipulation and reconstruction. The CT slices within the gage section were evaluated and post-processed. Fatigue tests were performed using a 22-kip MTS load frame. Data acquisition for the force data was collected by a MTS FlexTest60 controller. Strain was measured with DIC, and force measurements were taken from the MTS system; this was synchronized to images via a NI USB DAQ model 6212.

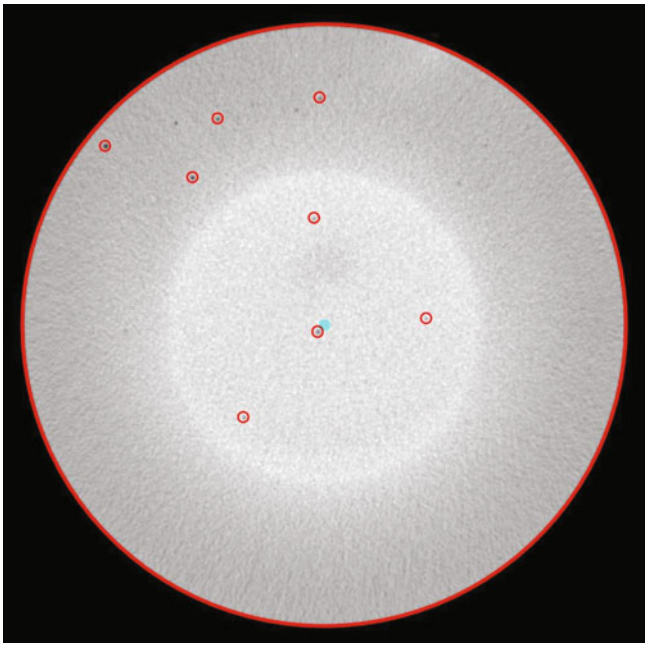

Fig. 5.3 Feature identification

5.2 Results and Discussion

An initial slice was identified for feature identification of the voids and can be seen in Fig. 5.3. The red circles in Fig. 5.3 indicate all the defects found in the image. The blue dot in the center of the image represents the center of the specimen. A border is also placed around the diameter of the specimen which is indicated by a red ring. Although it is best not to alter images to skew digital data, at times, brightness and contrast must be altered to obtain the data needed. However, the Feret diameter can be increased and decreased because of this.

By taking the data from each slice and manipulating the data in MATLAB, the porosity within the entire specimen can be obtained. Figure 5.4 shows the result of a mapping of the porosity radially normal to the z-axis. Figure 5.4 is porosity relative to edge distance in a polar coordinate system from the z-plane of a single specimen. Data of the average porosity size found from ImageJ in Table 5.1 for all as-built specimens.

Tammas-Williams proposed multiple rankings for stress intensity factors; a ranking of interest was selected from the multiple rankings. The failure location was estimated by using a simplistic version of the equation which includes the nonuniform stress due to the porosity position($\sigma_x(position)$), the stress concentration in relation to the surface distance ($K_t(surface)$), the pore aspect ratio ($K_t(AR)$), proximity to other pores ($K_t(proximity)$), and the area of a defect normal to the applied stress ($\sqrt[4]{A_n}$) [4]. The full equation can be seen in Equation 5.1.

$$\Delta K_I(relative) = \sigma_x(position)K_t(surface)K_t(AR)K_t(proximity)\sqrt[4]{A_n} \tag{5.1}$$

It is important to note that all the defects are assumed as round and spherical by shape; none are oblate. Because of this assumption, it can be shown by Biswal the aspect ratio will be 1.0 [5]. Therefore, the reduced equation is written as Equation 5.2 in the following.

$$\Delta K_I(relative) = K_t(surface)K_t(proximity)\sqrt[4]{A_n} \tag{5.2}$$

There are two other methods proposed and evaluated in this study. Equation 5.3 uses portions of the previous values from Equation 5.1 but additionally includes the length of the pore in the z-direction ($K_t(length)$) and the radius (r) of the pore. Therefore, Equation 5.3 considers the extra dimension within the defect damage criterion.

$$\Delta K_I(relative) = K_t(surface)K_t(proximity)K_t(length)r \tag{5.3}$$

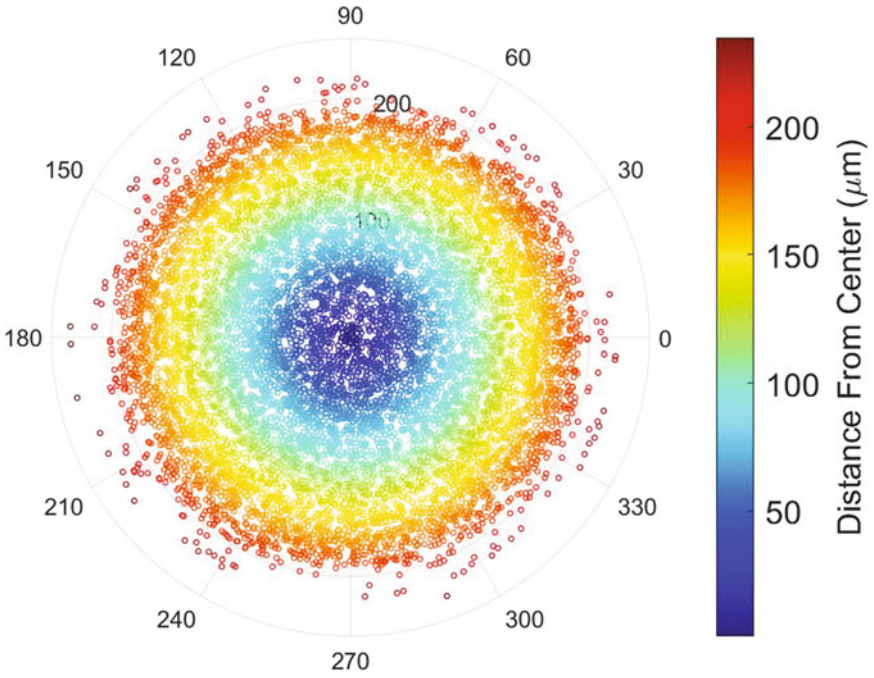

Fig. 5.4 Mapping of porosity

Table 5.1 Specimen porosity and life characteristics

Specimen name	Applied stress (MPa)	Fatigue cycle life (cycles)	Avg. Feret diameter (μm)	Estimated CT slice failure Loc.	CT slice failure Loc. (distance from closest estimation)
01-TT	689	5.08×10^3	58.07	902^4, 1091^4, 1758^2, 1758^3	784 (1759.5 μm)
04-TT	449.7	7.82×10^4	54.93	1062^2, 1062^3, 1899^4, 1916^4	1616 (4473.3 μm)
07-TB	689	13.02×10^3	57.93	339^4, 1798^4, 1826^2, 1827^1	1732 (1088.3 μm)
10-TT	499.5	2.66×10^4	57.95	328^3, 1002^4, 1166^4, 1597^2	1764 (2490.1 μm)

Lastly, a facile formula is used to produce a prediction of crack initiation location as Equation 5.4. Equation 5.4 only utilizes the distance from edge (ED) and radius of pore size (r). It is commonly known that defects in relation to the edge directly relate to the detriment of fatigue life. Additionally, defect/porosity size can also be a significant factor at times when determining the location of failure. Therefore, ED and the r will be used for the final prediction criterion.

$$\Delta K_I(relative) = (ED)r \tag{5.4}$$

The results from the fatigue tests can be found in Table 5.1 as well as the average Feret diameter of each specimen, the estimated CT slice locations from each defect damage criterion, and the identified CT slice failure location. The CT slice failure locations in Table 5.1 were found by identifying a strain field located on the specimen within VIC 3D. CT images were evaluated visually and were compared to the fracture surface captured on the microscope. The CT slice which aligned with the location of failure was documented. In Table 5.1 the different criterions are indicated by the estimated CT slice failure location value having a superscript number associated with each equation.

A correction was applied to locating the true CT image where failure occurred from DIC. The original CT slice estimation from DIC for each as-built specimen is shown in the following with the corrected value enclosed in parentheses: 01-TT CT = 797 (784), 04-TT CT = 1619 (1616), 07-TB CT = 1732 (1732), and 10-TT CT = 1750 (1764). The change of CT slice failure location was made by visually inspecting the fracture surface to that of the location CT scan images.

Figure 5.5 shows the fracture surface associated with specimen 04-TT. At the top of the image, a defect can be seen by its bright intensity compared to the rest of the specimen. This defect is the location of the crack initiation and is viewed as a gas pore caused during the EBM process. Shown in Fig. 5.6, the CT scan image of the determined failure location shows the same pore near the top-right edge of the specimen cross-section. The pore at the edge is the same crack initiation pore found from Fig. 5.5. The pore located was also witnessed in DIC and the crack can be seen in Fig. 5.8. The SN curve for the data

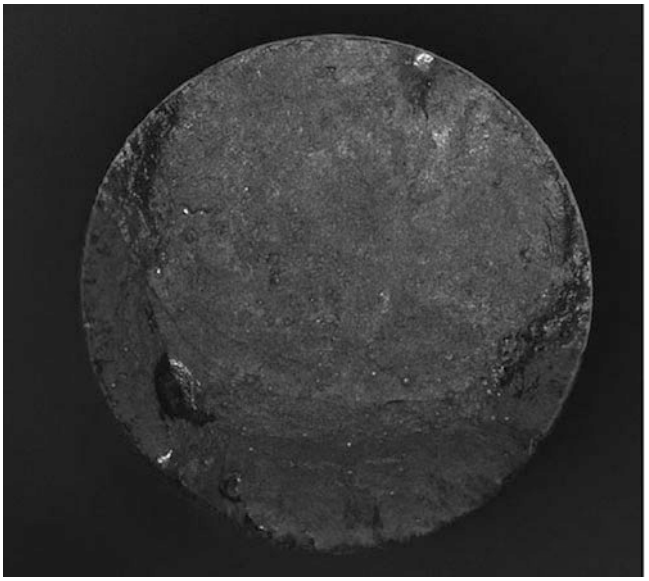

Fig. 5.5 04-TT Fracture surface

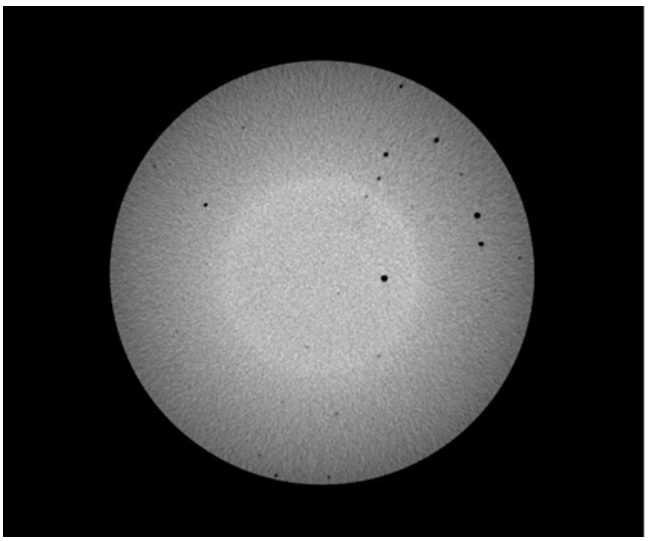

Fig. 5.6 04-TT Fracture CT image

tested is shown in Fig. 5.7. Majority of the specimens tested followed the 10% significance confidence interval presented in compared literature [6].

Shown in Fig. 5.8, specimen 04-TT is presented with a contour of the strain field, determined via DIC, after a crack has initiated. The spectrum of colors indicate the strain on the specimen where dark purple indicates 0.00245 and the dark red indicates 0.0088. However, the scale bar is not presented within Fig. 5.8 because of the discontinuity of the strain field due to the presence of the crack and therefore can only be utilized as a qualitative means of identifying localized deformation. This, however, demonstrates how the location for a crack was found.

CT images of Ti-6Al-4V were obtained and referenced to the speckle images from DIC and the fracture surface of the specimen, and thus a conclusion was made of where the specimen broke as well as the primary defect which ultimately led to crack initiation. From Table 5.1, it was found that Equation 5.4 yielded the closest predicted location of failure specimen 01-TT, 04-TT, and 07-TB and Equation 5.2 yielded the closest prediction for specimen 10-TT. All the prediction methods were able to approximate majority of the specimens failure location by using defect characteristics found from CT images within approximately 1–2 mm.

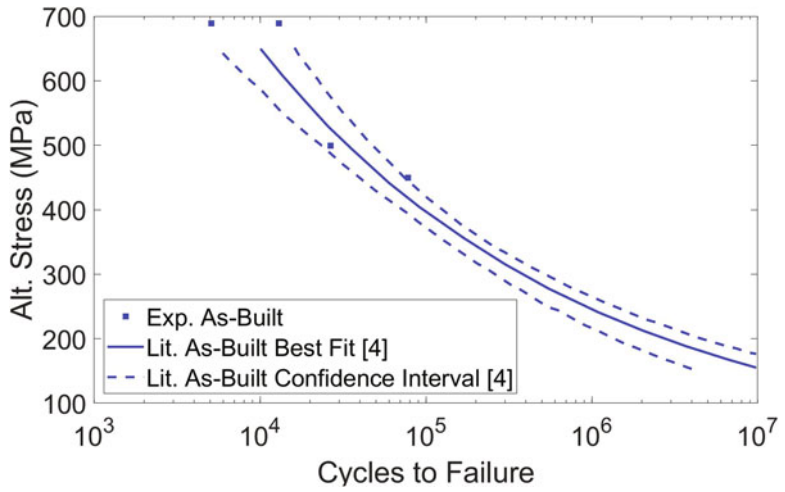

Fig. 5.7 Fatigue life results [4]

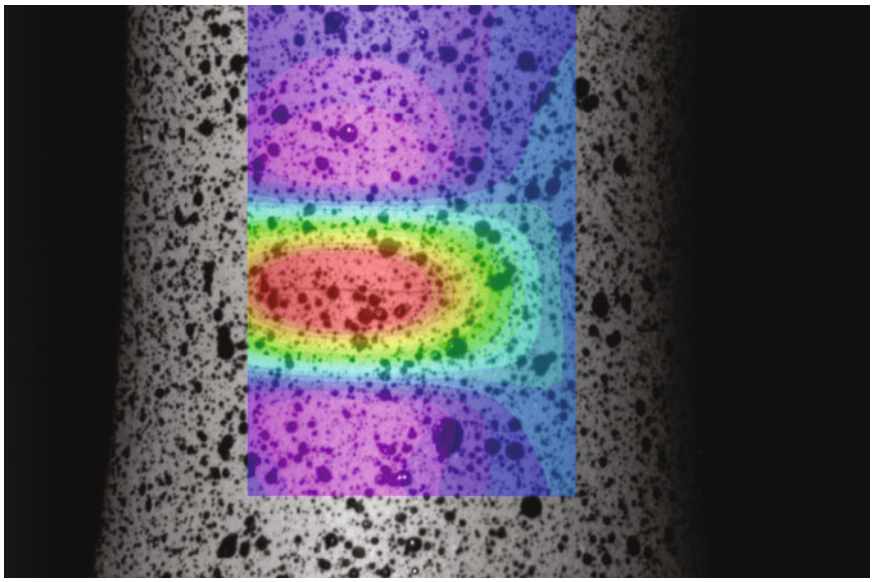

Fig. 5.8 04-TT DIC strain field

5.3 Conclusion

For the limited sample of specimens tested, the fatigue life has yielded similar SN behavior found in the literature and suspected to be of nominal material properties to other EBM as-built specimens. LOF caused a crack initiation for one specimen, causing fatigue life to be lower than expected.

- The location of the crack initiation can be estimated to a specific area, but there are various factors affecting the start of a crack which may not have been considered for future testing.
- By using multiple criterions, a prediction of failure can be found within 5,000 μm at most and is usually around 2,000 μm.
- The algorithms have the capability of improving, but they show great potential for detecting stress fields and failure points.
- LOF was detected throughout the specimens and ultimately caused a crack initiation for one specimen causing fatigue life to be lower than expected. This requires future work to identify LOF within CT images or by a different means to fully analyze all defects within in AM fabricated material.
- Equation 5.3 of the methods used to predict failure location performed the worst out of the three. This ultimately shows that the length does not have a significant impact on the failure location with respect to axial loading.

Acknowledgments The authors would like to thank the Turbine Engine Fatigue Facility of the Air Force Research Laboratory at Wright-Patterson Air Force Base for equipment use, assistance, and technical support of this research effort. The authors would also like to acknowledge and thank the Center for Design and Manufacturing Excellence at the Ohio State University for supplying and creating the material needed with their equipment.

References

1. Tofail, S.A., Koumoulos, E.P., Bandyopadhyay, A., Bose, L., O'Donoghue, S., Charitidis, C.: Additive manufacturing: scientific and technological challenges, market uptake and opportunities. Mater. Today **21**(1), 22–37 (2018)
2. Findlay, S., Harrison, N.: Why aircraft fail. Mater. Today **5**(11), 18–25 (2002)
3. Hrabe, N., Gnäupel-Herold, T., Quinn, T.: Fatigue properties of a titanium alloy (ti-6al-4v) fabricated via electron beam melting (ebm): effects of internal defects and residual stress. Int. J. Fatigue **94**, 202–210 (2017)
4. Tammas-Williams, S., Withers, P., Todd, I., Prangnell, P.: The influence of porosity on fatigue crack initiation in additively manufactured titanium components. Sci. Rep. **7**(1), 7308 (2017)
5. Biswal, R., Syed, A.K., Zhang, X.: Assessment of the effect of isolated porosity defects on the fatigue performance of additive manufactured titanium alloy. Addit. Manuf. **23**, 433–442 (2018)
6. Chern, A.H., Nandwana, P., Yuan, T., Kirka, M.M., Dehoff, R.R., Liaw, P.K., Duty, C.E.: A review on the fatigue behavior of ti-6al-4v fabricated by electron beam melting additive manufacturing. Int. J. Fatigue **119**, 173–184 (2019)